A Tracking System for Upstream Detectors in DIRAC

B. Adeva, A. Romero, O. Vázquez Doce

[a] *Santiago de Compostela University, Spain*

Abstract

This note describes the method used in DIRAC to perform:

a) pattern recognition of particle tracks using 11 detectors upstream the magnet.

b) matching with drift chamber tracks to determine the first order correction to pion momentum.

c) reconstruction of the longitudinal and transverse components of Q-vector in the center-of-mass frame, as well as their precision errors.

Because resolution in Q-vector components is ultimately limited by multiple scattering in the target foil and detector materials, special effort has been devoted to a precise mathematical description of particle correlations thereby induced, and to event-by-event covariance matrix calculation.

The results obtained allow identical resolution for prompt and accidental pairs in the analysis. Some unambiguous resolution and performance checks have been done using real data from the spectrometer.

DIRAC internal note 2003-08 *6 August 2003*

1 Introduction

The method described here is essentially present in the ARIANE reconstruction package since 2000, in what concerns the independent recognition of track elements upstream the magnet. A more recent upgrade has been introduced in relation with the handling of multiple scattering, which becomes of critical importance.

In fact, the method used is already described conceptually in reference [1], only the actual implementation with real stereo angles, and other setup parameters, remained to be done.

Preliminary studies presented within the experiment using Monte Carlo simulation, have clearly indicated that a better resolution in Q_X and Q_Y is obtained, by a factor of 2.5, with respect to other existing methods using only limited experimental information. Apart from the resolution problem, the method has the additional advantage that the copious background hits present in upstream detectors, due to the high beam intensity, can be unambiguously reduced by selection of only those that show a well defined probability to belong to a particle track. Moreover, the redundancy of particle trackers before the magnet allows to circumvent possible systematic effects in detector response, that might be extremely difficult to simulate by Monte Carlo.

2 Pattern Recognition

A program has been developed to perform standalone pattern recognition of stereo tracks in upstream detectors pointing to the beam intersection with the target.

An essential ingredient of this tracker is the use of the stereo angles $X^{'}$ $(+5^{o})$ and $Y^{'}$ (-5^{o}) of GEM/MSGC detector, and of the U-plane (45^{o}) of scintillation fibre detector (SFD), installed in 2002. A second key feature is the utilisation of the time markers provided by the TDC channels of SFD. Due to the intrinsic bandwidth limitation of the pipelined GEM/MSGC electronics (built in 1997), this detector actually receives pileup signals during a larger time interval (approximately $240ns$) than the standard coincidence gate of the experiment. Therefore one of the tasks of the pattern recognition is to provide a consistent timing for each track. This time mark will be matched later with that provided by the TOF counters, associated with drift chamber tracks.

The pattern recognition has two steps:

- identification of X and Y segments (hit pairs) in each projection separately, pointing towards the estimated beam intersection with the target. Single hits with no correspondance are also accepted as segments, with a slope defined by the interaction point
- association of X and Y segments to form a stereo track, when a corresponding hit is found in the extrapolation to one of the tilted planes $X^{'}$,$Y^{'}$, or U.

In order to minimise noise contributions while keeping efficiency close to maximum, the search windows at one σ in particle extrapolation (interpolation) from detector i to detector j [1] with $i < j$ ($i > j$), are calculated rather accurately during the previous two steps. A 3σ cut is then applied at each combination tried. The calculation of the search window receives contributions from two sources in quadrature : multiple scattering and angle subtended by the beam spot at detector i. For $i < j$, the former is determined by the expression:

$$\Delta r^2_{MS} = V_{MS}(i,i)\left(\frac{z_{i+1} - z_i}{z_i - z_T}\right)^2 + |V_{MS}(j,j) - V_{MS}(i,i)|$$

where $V_{MS}(i,i)$ are the diagonal elements of the matter component of covariance matrix defined in next section, and z_T is the Z-coordinate of the target. For a given beam spot size s_B, the uncertainty it causes in the extrapolation from detector i to j is given by: $\Delta r_B = s_B \left|\frac{z_i - z_j}{z_i - z_T}\right|$.

In order to define a track, a minimum of 4 hits is required among the 6 detectors (7 detectors, from 2002 onwards). In Fig. 1 we show the distribution of the number of tracks found per event by the pattern recognition, as well as the hit multiplicity per track.

3 Track Fitting

Once identified, the hits that belong to the track are fitted to a straight-line hypothesis A in order to determine the two slopes (x' and y') and intercepts (x_0 and y_0) of the particle trajectory at a given longitudinal coordinate z_0:

$$A = \begin{pmatrix} x_0 \\ x' \\ y_0 \\ y' \end{pmatrix}$$

[1] we assume detector numbers in increasing order from the interaction point

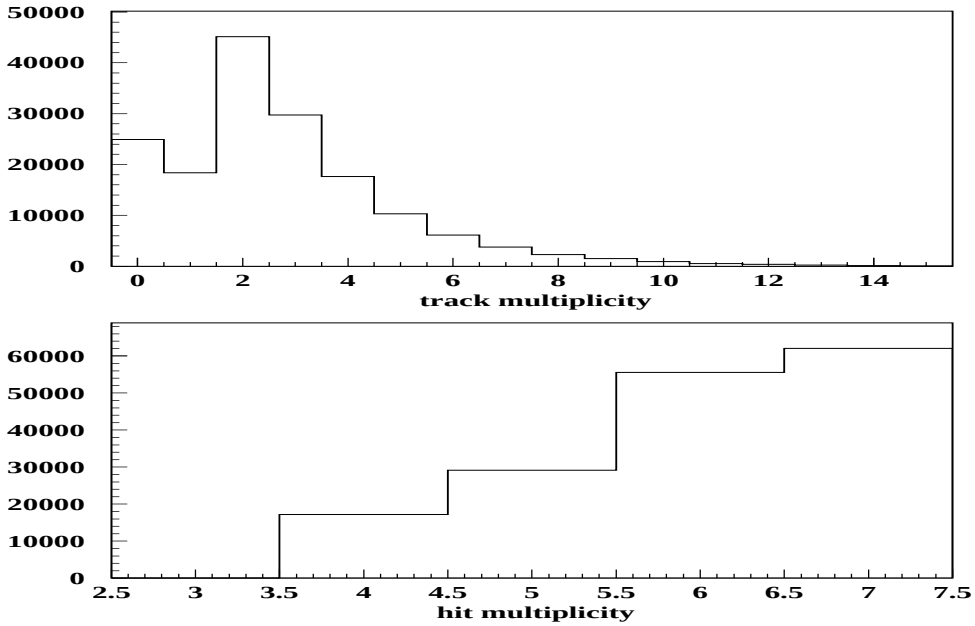

Fig. 1. *The top histogram shows the number of tracks found per event by the pattern recognition, and the bottom one the hit multiplicity (number of fired detectors) per track.*

The 4×4 covariance matrix of the previous fit for A is also determined, as well as the χ^2 and fit probability.

Due to the relatively small pion momenta, a fitting procedure has been developped that takes proper account of Coulomb multiple scattering in the covariance matrix, including detector-to-detector correlations implied by particle propagation. Full precision with this method can only be achieved once the particle momentum has been determined, and this will only happen at late stages of the ARIANE reconstruction, after matching with drift chamber tracks has been achieved.

In practice, an average particle momentum is used in a first iteration, which is later updated in successive re-fits. The procedure we shall describe is implemented in general form, in order to cope with $i = 1, N$ detectors located at

Z-coordinates z_i and measuring at arbitrary stereo angles θ_i. This geometrical information for upstream detectors is encoded by the matrix:

$$H = \begin{pmatrix} \cos\theta_1 & z_1\cos\theta_1 & \sin\theta_1 & z_1\sin\theta_1 \\ \cos\theta_2 & z_2\cos\theta_2 & \sin\theta_2 & z_2\sin\theta_2 \\ . & . & . & . \\ . & . & . & . \\ \cos\theta_N & z_N\cos\theta_N & \sin\theta_N & z_N\sin\theta_N \end{pmatrix}$$

The N measurements t_i for $i = 1, N$ are stored in the vertical array T in local coordinates of the corresponding detector. The χ^2 to be minimised is then given by the expression:

$$\chi^2 = (T - HA)^T (V_{det} + V_{MS})^{-1} (T - HA)$$

where $V = V_{det} + V_{MS}$ is the $N \times N$ detector covariance matrix. V_{det} is the diagonal matrix which describes intrinsic detector resolutions squared in each detector plane:

$$V_{det} = diag \left(\sigma_1^2, \sigma_2^2, \ldots, \sigma_N^2\right)$$

and V_{MS} is the non-diagonal correlation matrix that describes the random particle propagation through the detectors and passive materials due to Coulomb multiple scattering. We assume N thin detectors $i = 1, N$ numbered in ascending order from the interaction point, M_1 thin layers before detector 1 and M_2 layers located after detector N. The total number is scatterers is therefore $M = N + M_1 + M_2$.

The V_{MS} matrix encodes the information of the matter distribution seen by the particle which is observed by detectors i and j, and has traversed material thicknesses s_k of average radiation length X_{0k} each, located at coordinates z_k. For $i \leq j$ it is given by:

$$V_{MS}(i,j) = \sum_{k=1-M_1}^{i-1} \theta_{0k}^2 (z_i - z_k)(z_j - z_k)\cos^2(\theta_i - \theta_j) \qquad (1)$$

The sum extends over all material planes k seen by the particle from the interaction point up to the preceeding plane to detector i. The average multiple

scattering angle θ_{0k} in each layer depends on the particle momentum p (and velocity β) according to the expression:

$$\theta_{0k} = \frac{13.6 MeV}{p\beta c}\sqrt{\frac{s_k}{X_{0k}}}\left[1 + 0.038\ ln\left(\frac{s_k}{X_{0k}}\right)\right]$$

This matrix is symmetrised by construction: $V_{MS}(j,i) = V_{MS}(i,j)\ \forall\ i \leq j$. The relative orientation $\theta_i - \theta_j$ between detector planes i, j determines proper correlation between their respective measurements.

Note that, whereas V_{MS} is defined only for (active) detectors i, j, the sum in (1) runs over all material planes k present in the setup, whether they are instrumented detectors or no. In particular, the target and vaccuum chamber membrane thicknesses are included.

The minimum χ^2 fit A is obtained by matrix inversion :

$$A = \left(H^T(V_{det} + V_{MS})^{-1}H\right)^{-1}\left(H^T(V_{det} + V_{MS})^{-1}T\right)$$

where $V(A) = \left(H^T(V_{det} + V_{MS})^{-1}H\right)^{-1}$ is the 4×4 covariance matrix for the measurement of A.

Calculations are performed in double precision using standard CERNLIB routines for matrix manipulation. According to individual detector efficiencies, it is possible that a given detector does not show any hit along the track. It is to be noted that whereas unhit detectors i do not contribute directly to the calculation of χ^2 ($V^{-1}(i,j) = V^{-1}(j,i) = 0\ \forall j$ with $V = V_{det} + V_{MS}$), they do contribute to the correlation matrix of the active ones.

The previous fit is intended to provide the best measurement of the particle trajectory at the proton interaction point with the target. However, maximum resolution in the momentum determination requires the measurement be optimised at the magnet entrance, when used as input for the transfer function of the DIRAC dipole magnet. For this purpose, a calculation $\tilde{V}_{MS}$ for $i \leq j$ is performed in the following way, at the appropriate level of ARIANE program:

$$\tilde{V}_{MS}(i,j) = \sum_{k=j+1}^{M+M_2} \theta_{0k}^2 (z_i - z_k)(z_j - z_k)\cos^2(\theta_i - \theta_j) \qquad (2)$$

where k now runs over material planes located after detector j. As compared to V_{MS}, the matrix $\tilde{V}_{MS}$ actually describes the particle propagation over the M layers in reverse order, as if it propagated backward in time.

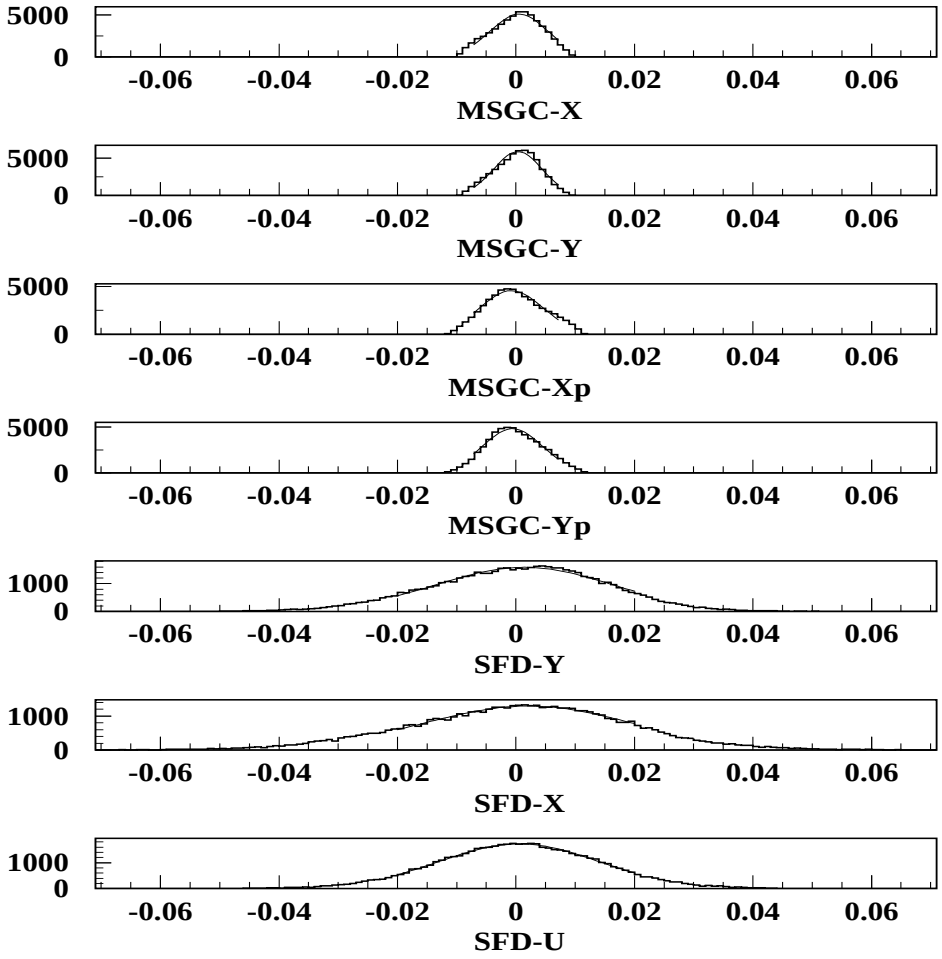

Fig. 2. *Distribution of distance between the fitted track extrapolation to a given detector plane and the actual measured coordinate in this plane (residuals). Detectors are shown in ascending order from the interaction point. Tracks with 7 hits are used.*

In Fig. 2 we show the track residuals observed in all GEM/MSGC and SFD detectors, with respect to the correlated fit. Intrinsic detector resolutions used are 60 μm for MSGC and 200 μm for SFD. The corresponding probability distribution is shown at the top part of figure 3.

In order to test the relative performance of the V_{MS} and $\tilde{V}_{MS}$ matrices, we have used as a test the Ionisation Hodoscope. Because the gaps in this detector are very small, and it is located far at the opposite end of the target, resolution in their location by the tracking system is dominated by the handling of multiple scattering, as momentum resolution is. Tracks going through the gaps are easily identified by requiring no visible signal on a given IH layer. A gausssian fit to the observed gap width yields sigma values of 479 $\pm$ 16 μm and 284$\pm$ 12 μm for the forward and backward fits, respectively.

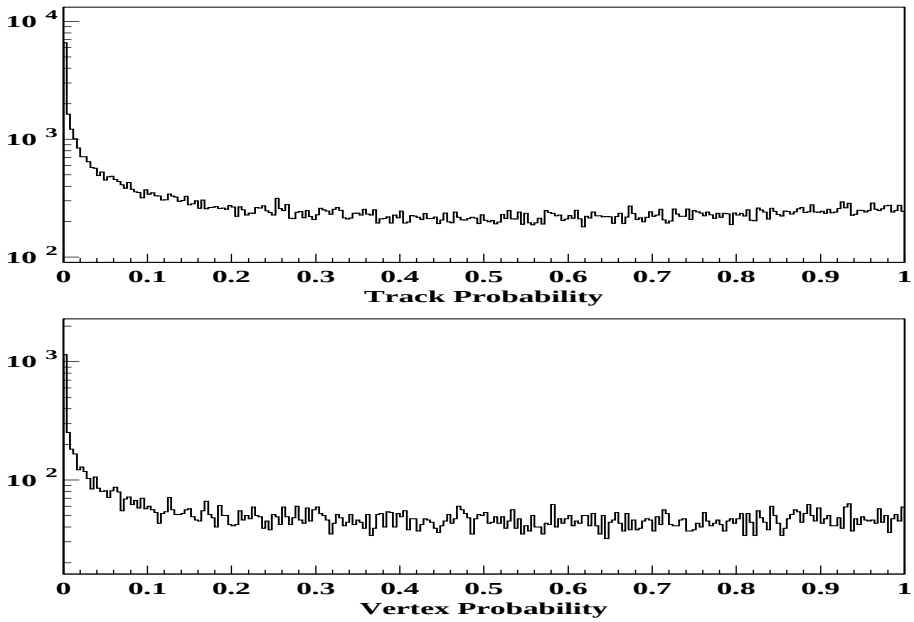

Fig. 3. *The top histogram shows the probability that the 7 hits found by the pattern recognition actually belong to a particle track, propagating with multiple scattering theory as described. No beam constraint is imposed by this fit. The bottom distribution corresponds to the probability that two tracks in a prompt pair, each with an arbitrary number of hits, have a common intersection at the target plane.*

4 Matching with Drift Chamber Tracks

For every opposite-charge pair, each track reconstructed in drift chambers is extrapolated backward by means of the transfer function of the DIRAC dipole magnet, using a first order momentum hypothesis based upon the calibrated X-coordinate of the beam. The extrapolated coordinates (x_1^{dc}, y_1^{dc}) and (x_2^{dc}, y_2^{dc}) obtained at a given reference plane (chosen to be the SFD-X detector) are then compared with those extrapolated forward for every ordered pair of upstream tracks (x_1^{up}, y_1^{up}) and (x_2^{up}, y_2^{up}). A minimum χ^2 test is used to select the pair of upstream tracks which provides best matching with the original charged-particle pair in drift chambers, according to the expression:

$$\chi^2 = \left(\frac{x_1^{up} - x_1^{dc}}{\Delta x_1}\right)^2 + \left(\frac{y_1^{up} - y_1^{dc}}{\Delta y_1}\right)^2 + \left(\frac{x_2^{up} - x_2^{dc}}{\Delta x_2}\right)^2 + \left(\frac{y_2^{up} - y_2^{dc}}{\Delta y_2}\right)^2$$

The values used for Δx_i and Δy_i are functions of momentum, given by parametrisations of the form $A + B/p$ in each case. The coefficients A and B were determined by fitting the dependence of the sigma values (gaussian fit) of the observed distances between drift chamber and upstream tracks, for X and Y

coordinates separately. Δx_1 (Δx_2) means that the function Δx is evaluated at track momentum $p = p_1$ (p_2), and the same for Δy.

Time cuts are applied for each track association prior to the χ^2 test, in order to ensure consistent time between corresponding upstream (t_{up}) and downstream (t_{dc}) tracks: $|t_{up} - t_{dc}| < \Delta t$, both for real and accidental pairs. Whereas t_{dc} is defined by the TOF counters, t_{up} is determined by the average of SFD TDC hits present. Cuts are also chosen according to the observed time-difference distributions.

It is clear that application of such time cuts produces a suppresion of the low-momentum proton background. The remainder of this background in the accidental pairs can be studied following the method introduced in reference [2], since also IH hits are incorporated to the track.

The differences between extrapolated coordinates from both sides of the magnet are shown in figure 4 for both X and Y. Figure 4 also shows the observed time differences between drift chamber tracks (determined by vertical hodoscopes) and upstream tracks (determined by SFD). Figure 5 is the their momentum dependence according to the parametrisations used.

Matching efficiency, defined as the fraction of drift chamber tracks that found correspondance with upstream detectors, is illustrated in Fig. 6 both for single tracks and for track pairs.

Cases in which the opposite-charge pair of drift chamber tracks can only be associated with a single (unresolved) upstream track, sufficiently close to both, are specially retained by the matching procedure. A double ionisation test will be applied to the track, based upon the observed pulses in Ionisation Hodoscope layers. In such configuration the time cuts are relaxed, in order to make acceptance for (unresolved) real and accidental pairs as close as possible.

5 Beam constraint and vertex fit

Once the track originally found by the pattern-recognition has been matched with a drift chamber track, its charge sign will be determined. Moreover, the magnitude of its momentum is improved with respect to the first-order approximation based upon the average beam position. For this purpose, the backward fit is used (see section 3), together with the magnet transfer function.

Knowledge of momentum will then allow a better description of multiple scattering in the covariance matrix, so a new track fit is performed. In addition, a general procedure is implemented to re-assign the original hits that belong to

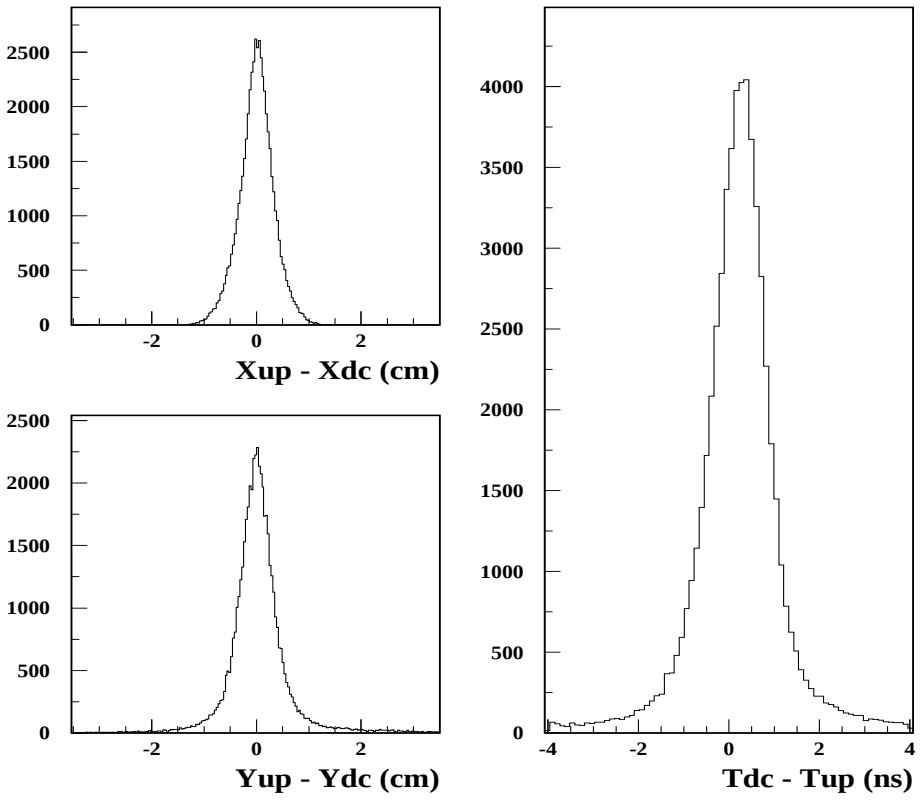

Fig. 4. *Top (bottom) left show the difference in X-coordinate(Y-coordinate) between backward-propagated drift chamber tracks (using first-order momentum by the magnet transfer function), and uptracks extrapolated to the matching plane. The right-hand histogram shows the time difference between DC tracks (as measured by the TOF counters, t_{dc}), and associated upstream tracks (t_{up}), as defined in section 2.*

the track. Individual hits found to be more than 3σ away from the (correlated) track are dropped, and track parameters are re-defined.

Track fitting based only upon measuring detectors provides in general a sufficient level of precision. However in those cases in which the track is left with only 4 hits, the fit has no degrees of freedom, and it becomes more vulnerable to noise hits. Two constraints are then introduced at the pattern-recognition level, requiring the center of the beam intersection with the target (X and Y coordinates) to lie on the particle trajectory, within a given probability cut. Mathematically, this is achieved by extending the detector covariance matrix dimension by two units. A tolerance at 1σ level is specified, corresponding to the observed beam spot size projections. Such a beam-constrained track re-fit is implemented in a general way, and it is actually performed at the final phase of the reconstruction, for tracks with an arbitrary number of hits.

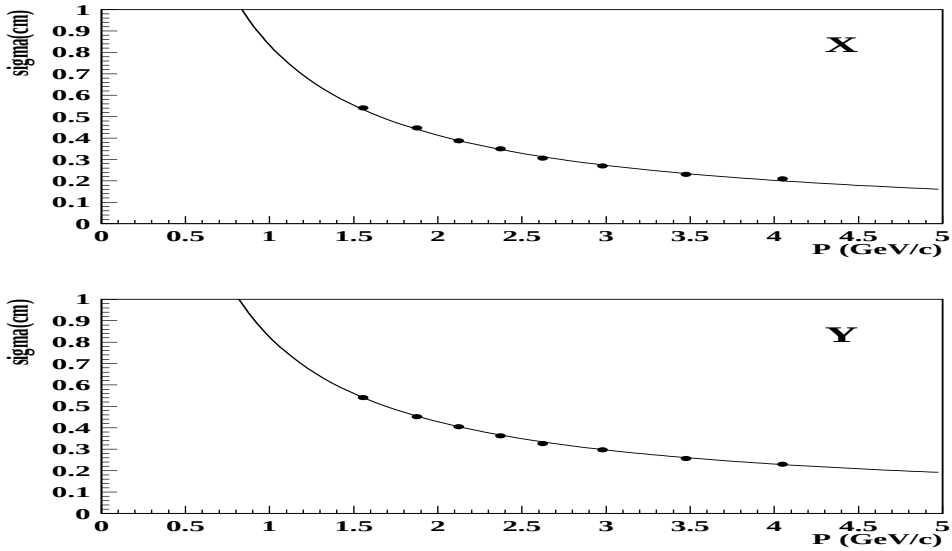

Fig. 5. *Top (bottom) figure shows momentum dependence of the fitted sigma values to the matching distances in X-coordinate (Y-coordinate) as shown in average in figure 4. The corresponding parametrisations $A + B/p$ are drawn in each case.*

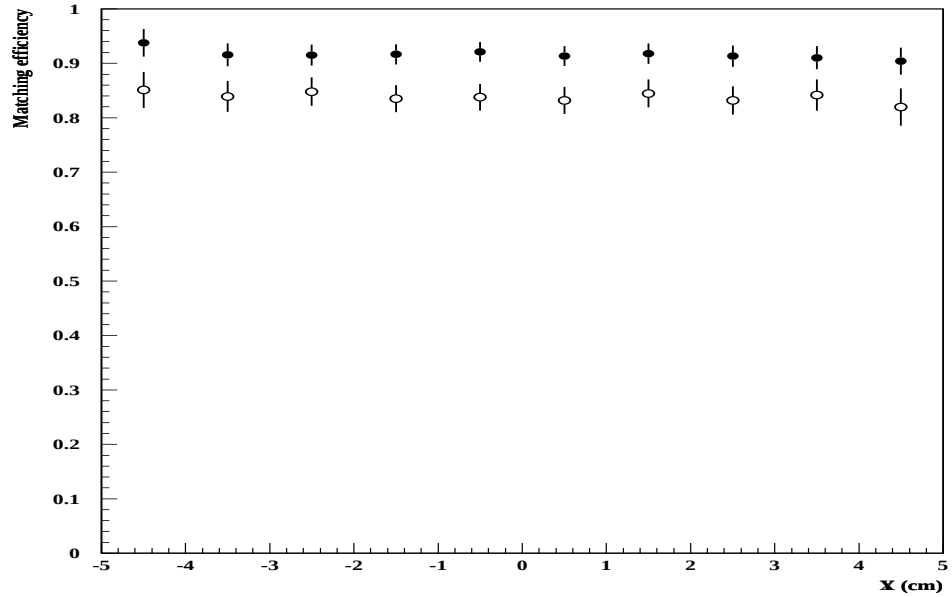

Fig. 6. *Fraction of drift chamber tracks which found a corresponding upstream track (black circles), as function of X-coordinate measured at the matching plane (SFD-X). Open circles show the fraction of opposite-charge pairs which found a corresponding pair of upstream tracks, as explained in the text.*

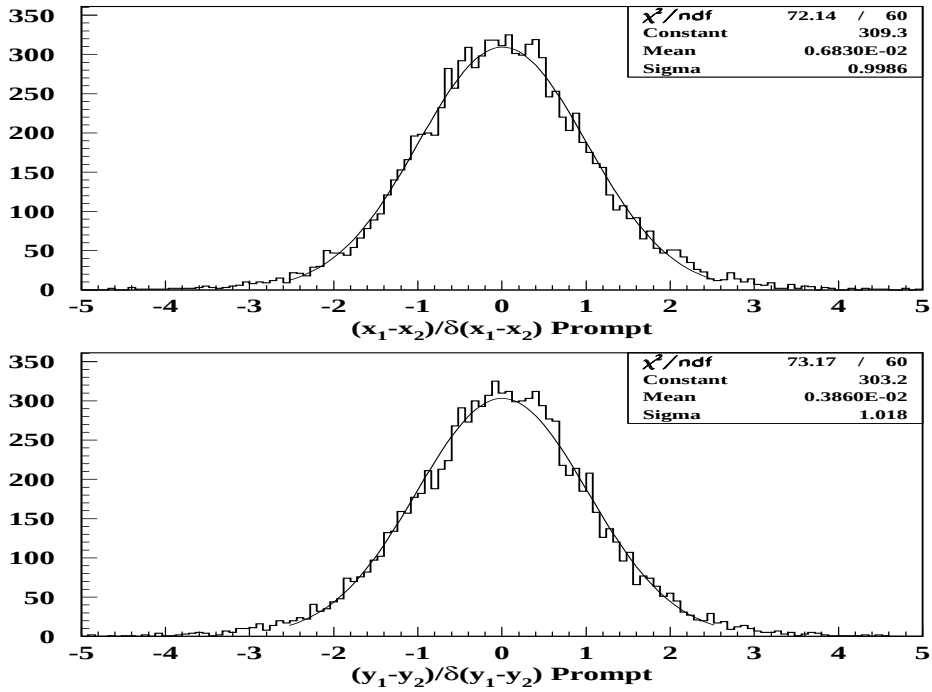

Fig. 7. *The top histogram shows the distribution of measured values of* $x_1 - x_2$ *divided by its error, where* x_1 *and* x_2 *are the X-coordinates of the positive and negative track intersections with the target plane. The error has been determined event-by-event by the beam-constrained fit. At the bottom the corresponding distribution is shown for the Y-coordinates. Only prompt pairs have been selected in these distributions.*

When individual tracks are subject to the beam-constrained fit, the target radiation length needs to be taken into account, in addition to the estimated beamspot size in X and Y projections. This input allows to extend the 7×7 detector correlation matrix $V = V_{det} + V_{MS}$ (as defined in section 3) to dimension 9×9. The track covariance matrix $V(A)$ then obtained trully represents the particle propagation at the target interaction point.

In order to illustrate the correctness of the error description provided by this procedure, we show in figure 7 the measured distribution of the differences between extrapolated track coordinates at the target plane, normalised to their calculated error (given by the diagonal elements of $V(A)$). It can be appreciated that there is perfect agreement between the calculated errors and the measured ones.

It is clear that the beam constraint, as we have defined it, is in better agreement with the hypothesis that both particles really come from the same interaction point. This is why we have determined the distributions in figure 7 only for prompt pairs. Accidental pairs, on the other hand, are only approximately described by this hypothesis. When we determine the distributions in figure 7

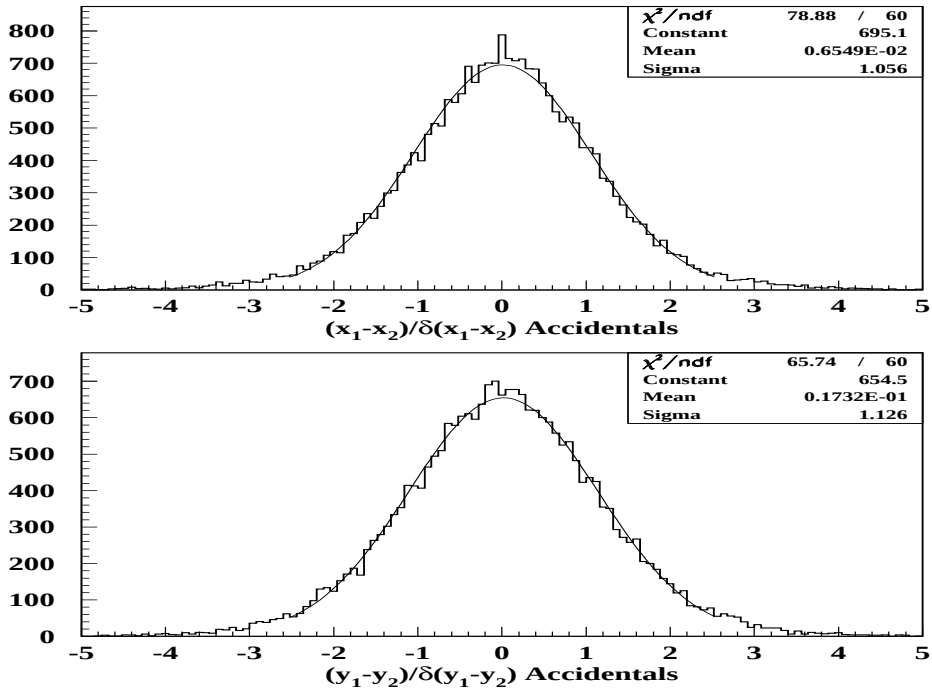

Fig. 8. *The contents of this figure are the same as those of figure 7, except that accidental pairs have been selected in this case. A precise description of the errors could only be achieved by decreasing the nominal sizes of the beam profile by 10% in X (20% in Y) in the beam-constrained fit.*

for accidental pairs with the same setting of beamsize parameters , we observe that the measured/calculated ratios increase to 1.07 and 1.14 in the X and Y projections, respectively. Equivalently, we obtain a good error match by artificially decreasing the nominal beamsize constraints in the fit in accordance to the indicated factors. When this is done, we obtain the distributions shown in figure 8. This prescription ensures equally precise error handling for real and accidental pairs, in the determination of Q_X,Q_Y and Q_L.

The beamsize dimensions that provide optimal description of the errors are consistent with those reported in reference [3], namely 1.0 mm and 1.7 mm in the X and Y projections, respectively. More direct evidence for the observed difference between real and accidental pairs can be obtained by comparing the measured sigma values of $x_1 - x_2$ ($y_1 - y_2$) as defined in figure 7 (8). They significantly differ by 6.5% (10.5%). The precise values obtained are indicated in table 1.

Table 1
Results of sigma values from gaussian fits to $x_1 - x_2$ and $y_1 - y_2$ using the beam-constrained fit, for prompt and accidental pairs separately. Indicated errors are statistical only.

	Prompt	Accidental
$x_1 - x_2$	1754 ± 18 μm	1884 ± 14 μm
$y_1 - y_2$	1870 ± 20 μm	2082 ± 16 μm

6 Alignment procedure

High precision in relative pion momentum components in the two-particle center-or-mass frame (Q_L, Q_X, Q_Y) can only be achieved after proper alignment between detector elements of the upstream detectors, the beam, and the drift chambers. In particular, a good description of track probabilities, multiple scattering correlations, and intrinsic detector resolutions requires this as a first step.

The alignment program can be carried out almost entirely using properly selected upstream tracks. The following 18 parameters have been determined as output of the calibration procedure:

- 7 offsets of individual detector planes in the direction perpendicular to the corresponding strips or fibres (position of the *first strip*).
- 7 Euler rotations of each detector plane about the Z-axis (precision tuning of the θ_i angles).
- mean position in X and Y of the beam center, with respect to the upstream detectors.
- overall Euler rotations about the Z and Y axis of uptream detectors as a whole with respect to drift chambers.

The first two items have been determined in a standard way, by dropping individual detector hits from the fit, and studying their observed residuals. An iterative procedure is then defined.

The third item (beamspot position) has been obtained by making a gaussian fit to the (unconstrained) intersection of fitted tracks with the target plane. The values are shown in table 2 for run 4745 in 2002, as illustration.

Not included in the previous list are the mean values of the interaction point in X and Y coordinates, the former being used to determine the first-order momentum hypothesis. These parameters depend on the relative alignment of the drift chambers with respect to the beam, and they can be determined independently of upstream detectors by assuming charge conjugation invariance

Table 2
Measured positions of the beam center, as seen by the upstream tracks in run 4745. Particle dispersion with respect to it is also shown, from the fitted sigma values. Errors shown are statistical only.

	X	Y
Mean	1645 ± 10 μm	-1759 ± 17 μm
Sigma	1989 ± 12 μm	2531 ± 10 μm

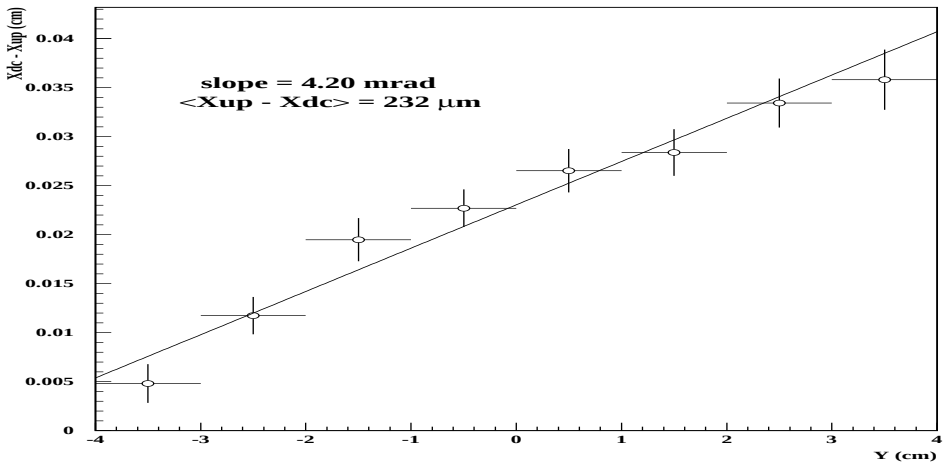

Fig. 9. *Measured offset in X-coordinate between drift chamber and upstream tracks at the matching plane, as function of Y-coordinate. Observed slope and intercept are indicated.*

in $\pi^+\pi^-$ interactions. Their values can be cross-checked with the mean offsets in X and Y observed in the matching procedure.

As illustration, we show in figure 9 the measured offset in X-coordinate between the drift chamber and the upstream tracks at the matching plane, as function of Y-coordinate. The observed slope of 4.2 mrad, measured in a particular run (4745), determines an overall Euler rotation about the Z-axis between the upstream detectors and the average of positive and negative arms. Slope and intercept are used as a correction when particle momentum is re-fit after matching with DC tracks.

7 Pulse-height in Ionisation Hodoscope

Straight-line tracks reconstructed in the upstream detectors are extrapolated to the Ionisation Hodoscope (IH), in order to determine the slab numbers

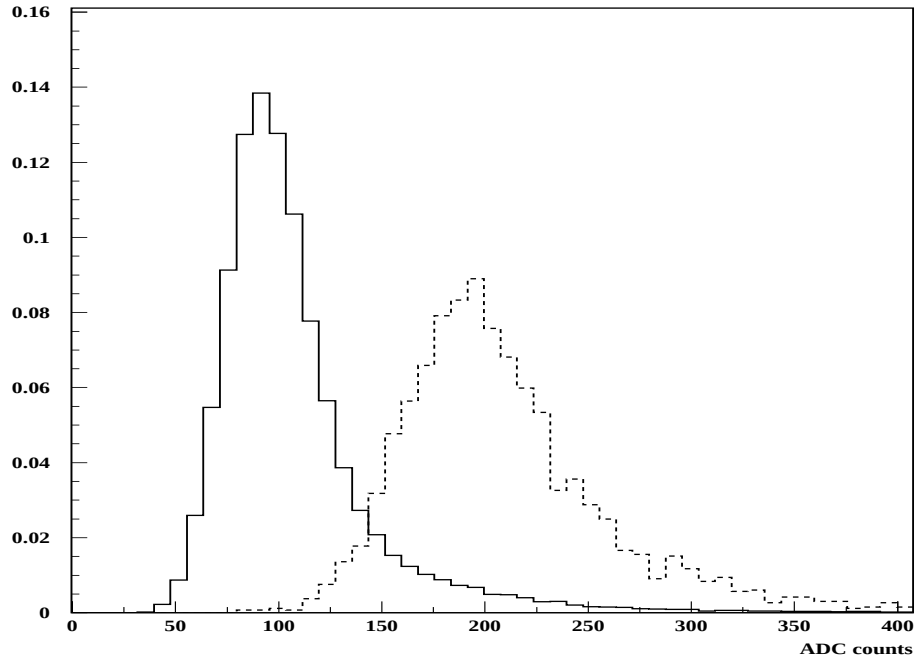

Fig. 10. *Pulse-height distribution observed in single slabs of Ionisation Hodoscope (XA layer) in two distinct selection cases for upstream tracks: only one track crossing the slab (continuous line) and two tracks crossing the same slab (dotted line).*

intersected by the particle at each detector plane. Pulse-height (ADC) and TDC information are incorporated to the track, after application of various corrections following reference [4], some of which depend upon the longitudinal coordinate along the counters.

Special attention is devoted at this point to unresolved tracks, in order to establish or not their two-particle nature by looking for a double ionisation signal in IH detector. Apart from Coulomb and pionium pairs, such unresolved tracks are expected to be found also from accidental pairs, in a proportion that we want to evaluate precisely.

The algorithm applied consists of excluding the maximum and the minimum pulses among those found in IH layers, and then require $A > A_{cut}$ with A being the average of the remaining ones. The cut value A_{cut} is optimised according to the fitted curves obtained for single and double track intersections on individual counters. It is remarkable that practically no background from single ionisation is observed, when two-track crossings are required on individual slabs, as it can be seen in the dotted line of figure 10.

References

[1] M. Pentia and S. Constantinescu, "Uncertainties induced by multiple scattering in upstream detectors of the DIRAC setup", DIRAC Note 2001-04.

[2] S. Trusov, "Proton to pion ratio in accidental coincidences", DIRAC Note 2002-10.

[3] A. Lanaro, "DIRAC beam parameters", DIRAC Note 2002-02.

[4] V. Brekhovskikh at al., "New Ionisation Hodoscope: design and characteristics", DIRAC Note 2002-09.